The Astrophysical Journal Letters, 878:L23 (7pp), 2019 June 10 https://doi.org/10.3847/2041-8213/ab263a
© 2019. The American Astronomical Society. All rights reserved.

The Supersonic Project: Shining Light on SIGOs—A New Formation Channel for Globular Clusters

Yeou S. Chiou[1,2], Smadar Naoz[1,2], Blakesley Burkhart[3,4], Federico Marinacci[5,6], and Mark Vogelsberger[7]
[1] Department of Physics and Astronomy, University of California, Los Angeles, CA 90095, USA; yschiou@physics.ucla.edu
[2] Mani L. Bhaumik Institute for Theoretical Physics, Department of Physics and Astronomy, UCLA, Los Angeles, CA 90095, USA
[3] Department of Physics and Astronomy, Rutgers, The State University of New Jersey, 136 Frelinghuysen Road, Piscataway, NJ 08854, USA
[4] Center for Computational Astrophysics, Flatiron Institute, 162 Fifth Avenue, New York, NY 10010, USA
[5] Department of Physics & Astronomy, University of Bologna, via Gobetti 93/2, I-40129 Bologna, Italy
[6] Harvard-Smithsonian Center for Astrophysics, 60 Garden Street, Cambridge, MA 02138, USA
[7] Department of Physics and Kavli Institute for Astrophysics and Space Research, Massachusetts Institute of Technology, Cambridge, MA 02139, USA
Received 2019 April 10; revised 2019 May 31; accepted 2019 May 31; published 2019 June 12

Abstract

Supersonically induced gas objects (SIGOs) with little to no dark matter (DM) component are predicted to exist in patches of the universe with non-negligible relative velocity between baryons and the DM at the time of recombination. Using AREPO hydrodynamic simulations we find that the gas densities inside of these objects are high enough to allow stars to form. An estimate of the luminosity of the first star clusters formed within these SIGOs suggests that they may be observed at high redshift using future *Hubble Space Telescope* and *James Webb Space Telescope* observations. Furthermore, our simulations indicate that SIGOs lie in a distinct place in the luminosity–radius parameter space, which can be used observationally to distinguish SIGOs from DM hosting gas systems. Finally, as a proof-of-concept, we model star formation before reionization and evolve these systems to current times. We find that SIGOs occupy a similar part of the magnitude–radius parameter space as globular clusters (GCs). These results suggest that SIGOs may be linked with present-day metal-poor local GCs. Because the relative velocity between the baryons and DM is coherent over a few Mpc scales, we predict that if this is the dominant mechanism for the formation of GCs, their abundance should vary significantly over these scales.

Key words: cosmology: theory – galaxies: high-redshift – methods: numerical

1. Introduction

The puzzling origins of globular clusters (GCs) have been greatly debated over the years (Gunn 1980; Peebles 1984; Ashman & Zepf 1992; Harris & Pudritz 1994; Grillmair et al. 1995; Moore 1996; Bromm & Clarke 2002; Kravtsov & Gnedin 2005; Mashchenko & Sills 2005; Saitoh et al. 2006; Muratov & Gnedin 2010; Bekki & Yong 2012; Kruijssen 2015; Renaud et al. 2017; Mandelker et al. 2018). These objects serve as the testing grounds for early structure formation because they are very old (∼13 Gyr, e.g., Trenti et al. 2015). For example, they have even been used to estimate the age of the universe (Krauss & Chaboyer 2003). Observations suggest that GCs contain practically no gravitationally bound dark matter (DM; e.g., Heggie & Hut 1996; Bradford et al. 2011; Conroy et al. 2011; Ibata et al. 2013, although see Taylor et al. 2015 for evidence to the contrary). Although direct observations of high-redshift GCs is difficult, statistical studies with strong gravitational lensing have enabled the investigation of high-redshift star-forming GC candidates (e.g., Elmegreen et al. 2012; Vanzella et al. 2017). There has even been some direct evidence of possible GC progenitors (e.g., Vanzella et al. 2016, 2019; Bouwens et al. 2017). Furthermore, GCs and their progenitors may also play a large role in reionizing the universe (e.g., Schaerer & Charbonnel 2011; Boylan-Kolchin 2018). The upcoming *James Webb Space Telescope* (*JWST*) offers an exciting chance to observe GCs and their progenitors at early times. These observations will give insight to the formation of the very early building blocks in the universe.

In the standard model of structure formation, due to the baryon-radiation coupling, baryon over-densities at the time of recombination ($z \sim 1020$) were about 5 orders of magnitude smaller than DM over-densities. Tseliakhovich & Hirata (2010) showed that not only were the amplitudes of the DM and baryonic density fluctuations different at early times (e.g., Naoz & Barkana 2005), but so were their velocities. After recombination, the baryons decoupled from the photons and their subsequent evolution was dominated by the gravitational potential of the DM. In the period following recombination, the baryons underwent rapid cooling. At this point, their relative velocity with respect to the DM, which at recombination was of the order of ∼30 km s^{-1}, became supersonic. Tseliakhovich & Hirata (2010) also showed that this relative velocity between the baryons and the DM remained coherent on scales of a few Mpc, and in these regions it can be modeled as a stream velocity.

The stream velocity effect has previously been overlooked because the velocity terms are formally second order in perturbation theory and are therefore neglected in the linear approximation. However, this second-order effect is unusually large, resulting in the non-negligible suppression of power at mass scales that correspond to the first bound objects in the universe (Tseliakhovich et al. 2011). The nonlinear effects of the stream velocity on the first structures were subsequently investigated using numerical simulations (e.g., Greif et al. 2011; Maio et al. 2011; Naoz et al. 2011, 2012; Stacy et al. 2011; Fialkov et al. 2012; O'Leary & McQuinn 2012; Richardson et al. 2013; Tanaka & Li 2014). The stream velocity also has significant implication on the redshifted cosmological 21 cm signal (e.g., Dalal et al. 2010; McQuinn & O'Leary 2012; Visbal et al. 2012), the formation of primordial black holes (e.g., Tanaka et al. 2013; Latif et al. 2014; Tanaka & Li 2014; Hirano et al. 2017; Schauer et al. 2017), and even

for primordial magnetic fields (Naoz et al. 2013). See Fialkov (2014) for a detailed review.

Recently, Naoz & Narayan (2014) proposed that metal-poor GCs may be linked to objects that can be formed without DM in the early universe in the presence of the stream velocity. These supersonically induced gas objects (SIGOs) were later found in numerical simulations by Popa et al. (2016) and Chiou et al. (2018). However, their connection to GCs is still uncertain. Specifically, the ability of SIGOs to form stars was not addressed in those simulations. If these objects indeed form stars, these first star clusters will host little to no DM component.

The formation of the first stars from pristine gas was addressed in length in the literature focusing on the detailed chemistry and equation of state (e.g., Abel et al. 2002; Bromm & Clarke 2002; Reed et al. 2005; Yoshida et al. 2006; Stacy et al. 2011; Glover 2013; Xu et al. 2016; Sarmento et al. 2018; Schauer et al. 2019). In this Letter we take a global, statistical approach through an investigation of the conditions for star formation in SIGOs via a simple density threshold argument. In particular, stars will form if the global gas density within a given SIGO is above the predicted critical value for star formation in pristine and low-metallicity gas (e.g., Christlieb et al. 2002; Krumholz & McKee 2005; Burkhart & Mocz 2018). We then use semi-analytical calculations to determine the luminosities of objects in our simulations. We note that, although we study these objects at $z = 20$, they still exists at lower redshifts (e.g., Naoz & Narayan 2014; Popa et al. 2016; Chiou et al. 2018). Thus, their expected luminosities could possibly be detectable with *JWST*.

This Letter is organized as follows: we begin by describing our simulations in Section 2 then we discuss the star formation model (Section 3) and the subsequent luminosity (Section 4). Finally we offer our discussion and qualitative predictions in Section 5.

2. Simulation Details and Object Classification

We run two cosmological simulations with the moving-mesh code AREPO (Springel 2010) in a 2 Mpc box with 512^3 DM particles of mass $M_{\rm DM} = 1.9 \times 10^3\ M_\odot$ and 512^3 Voronoi mesh cells with $M_{\rm gas} = 360\ M_\odot$. One run has a stream velocity value of $v_{\rm bc} = 2\sigma_{v_{\rm bc}}$, where $\sigma_{v_{\rm bc}}$ is the rms value of the stream velocity (i.e., the relative velocity between the gas and the DM component), while the other, which we use for comparison, has no such stream velocity. Both runs include radiative cooling (see Y. S. Chiou et al. 2019, in preparation). The cooling module in AREPO is based on a self-consistent primordial chemistry and cooling network, which includes the evolution of species H, H^+, He, He^+, He^{++}, and e^- in equilibrium with a photoionizing background that is spatially constant but redshift dependent. The gas cooling and heating rates are calculated as a function of redshift, gas density, temperature, and (for the metal line part) metallicity[8] See (Vogelsberger et al. 2013, and references therein) for further details on the numerical implementation of these processes. The simulations do not include explicit star formation or feedback.

We note that our simulations do not include H_2 cooling. Molecular cooling was shown to be important for early star formation (e.g., Hartwig et al. 2015; Glover & Jappsen 2007; Schauer et al. 2017, 2019). Nonetheless, the densities in our simulations (as we show below) reach the necessary high densities and low temperatures to trigger star formation. Thus, inclusion of molecular cooling in follow-up simulations will yield even higher densities, further facilitating star formation.

The initial conditions adopted different transfer functions for the DM and baryon components as described in Naoz & Barkana (2005) and Naoz et al. (2009, 2011, 2013, 2012). The runs were performed from a redshift of $z = 200$ to $z = 20$. The stream velocity is implemented as a uniform boost for the gas in the x-direction. The choice of $v_{\rm bc} = 2\sigma_{v_{\rm bc}}$ allows us to gain a larger effect; however, the same physical picture is applicable for $v_{\rm bc} = 1\sigma_{v_{\rm bc}}$, (as noted by Naoz & Narayan 2014). Furthermore, we gain more statistical power by adopting $\sigma_8 = 1.7$ (e.g., Popa et al. 2016; Chiou et al. 2018; Y. S. Chiou et al. 2019, in preparation).

We follow the structure definitions suggested in Chiou et al. (2018). In particular, DM-primary/gas-secondary (DM/G) objects are spherical overdensity DM halos that also contain gas. The gas-primary objects are gas objects obtained through running a friends-of-friends (FOF) algorithm on only the gas component and subsequently fitted to a tight ellipsoid. Both DM/G and gas-primary objects are identified by using the FOF algorithm with a linking length of 0.2 times the mean particle separation. Finally, the SIGOs are gas-primary objects that are outside the virial radius of the closest DM halo and also have gas fractions greater than 40%. These objects have little to no DM component. The advantage of our small simulation box is that it allows us to resolve SIGOs; however, it prevents us from following the detailed evolution of SIGOs to smaller redshift. Thus, in order to investigate the evolution of SIGOs at $z < 20$ we employ semi-analytical modeling. Throughout this Letter we assume a ΛCDM cosmology with $\Omega_\Lambda = 0.73$, $\Omega_m = 0.27$, $\Omega_B = 0.044$, $\sigma_8 = 1.7$, and $h = 0.71$. All the quantities that we analyze in this Letter are expressed in physical units.

3. Star Formation Model

We estimate the plausibility that a dense gas clump (either a SIGO or within a DM/G) may form stars. Primordial star formation may be the most suitable epoch during the evolution of the universe for the application of the Jeans criterion as the level of turbulence and strength of the magnetic field are expected to be significantly lower (Bromm et al. 1999, 2002). The Jeans criterion (Jeans 1902) and the related Bonnor-Ebert mass describes the balance between gravity and thermal pressure and is given by

$$M_{\rm BE} = 1.18\frac{c_{\rm s}^3}{\sqrt{G^3\rho}} = \frac{1.18}{\pi^{3/2}}\rho\lambda_{\rm J}^3, \quad (1)$$

where $c_{\rm s}$ is the isothermal sound speed in the region, G is the gravitational constant, ρ is the density of the gas, and $\lambda_{\rm J}$ the Jeans length. The mass in Equation (1) is the largest mass that an isothermal gas sphere embedded in a pressurized medium can have while still remaining in hydrostatic equilibrium (Ebert 1955; Bonnor 1956). This depends on the Jeans length, defined as follows:

$$\lambda_{\rm J} = \sqrt{\frac{\pi c_{\rm s}^2}{G\rho}}. \quad (2)$$

[8] Note that while all cooling rates include self-shielding corrections, these corrections do not apply above redshift of 6, and thus do not contribute for the cooling of the $z = 20$ objects.

The Jeans length is therefore the critical radius of a cloud where thermal energy is counteracted by gravity.

Because we are dealing with a supersonic medium, the other length scale of interest for defining a critical density for star formation is the sonic scale[9]:

$$\lambda_s = \left(\frac{L_{\rm drive}}{\mathcal{M}^2}\right). \quad (3)$$

λ_s is defined as the length scale such that $\sigma_l = c_s$, $\mathcal{M}$ is the Mach number on the driving scale, $L_{\rm drive}$, of the turbulence, and σ_l is the one-dimensional velocity dispersion computed over a sphere of diameter l within a turbulent medium. The sonic scale physically represents the scale at which turbulence in the gas transitions from supersonic to subsonic.

As discussed in Krumholz & McKee (2005), if $\lambda_J \leqslant \lambda_s$, gravity is approximately balanced by thermal plus turbulent pressure, and the object is at best marginally stable against collapse. Here we assume that the magnetic field is dynamically unimportant relative to turbulence and gravity. If $\lambda_J \gg \lambda_s$, turbulent/thermal kinetic energy greatly exceeds gravitational potential energy and the object is stable against collapse. As λ_J is a function of the local density, the condition $\lambda_J \leqslant \lambda_s$ for collapse translates into a minimum local density required for collapse (in the absence of magnetic fields). Equating the two length scales yields a critical density

$$\rho_{\rm crit} = \frac{\pi c_s^2 \mathcal{M}^4}{G L_{\rm drive}^2}, \quad (4)$$

which can be rewritten in terms of the virial parameter, and assuming that the driving scale of the turbulence is the characteristic diameter of the cloud, i.e., $L_{\rm drive} = L_{\rm cloud}$, as

$$\rho_{\rm crit} = \frac{\pi^2}{15}\rho_0 \alpha_{\rm vir,l} \mathcal{M}^2, \quad (5)$$

where $\alpha_{\rm vir,l} = 5\sigma_l^2 L_{\rm cloud}/(2GM_{\rm cloud})$, the ratio of turbulent to gravitational energy. We note that these equations are only meaningful in the presence of a supersonic flow, as in our case.

In this simple stability picture, once the critical density is reached, the gas becomes unstable to gravitational collapse. Burkhart & Mocz (2018) related the critical density to a transition density between a piecewise lognormal and power law of the density distribution. A power-law density probability distribution function (PDF) is the 1-point statistic's signature of gravitational collapse, regardless of the gas metallicity. A turbulent medium will have an initially lognormal density distribution, but once gravitational collapse sets in, the distribution can be described by a power law (Girichidis et al. 2014; Burkhart et al. 2017; Guszejnov et al. 2018). Thus, the transition density as a critical density for collapse is a natural consequence of the density distribution function. Below, we adopt this critical density threshold as a star formation indicator.

We apply the above star formation criterion to the objects found in the simulation. In Figure 1, we show the density of representative star-forming SIGOs normalized to their critical density for star formation. To compute the critical density we need an estimate of the turbulence sonic scale, which is given by $L_{\rm cloud}/\mathcal{M}^2$ (e.g., Burkhart 2018). Because SIGOs are ellipsoidal (e.g., Chiou et al. 2018), we assume $L_{\rm cloud} \sim 2R_{\rm max}$, because this is the maximum scale at which turbulence can be generated. We calculate the critical densities for each object type (i.e., DM/Gs and SIGOs) in our simulations following Equation (4). Considering first the DM/G objects we find that at $z = 20$, 19% (85%) of them have densities and temperatures that yield favorable conditions for star formation for the $2\sigma_{v_{\rm bc}}$ ($v_{\rm bc} = 0$) run. This difference between the stream velocity and no stream velocity case is expected as the stream velocity effect reduces the gas fraction of DM halos (e.g., Tseliakhovich et al. 2011; Naoz et al. 2012). In Figure 2 we show the temperatures and densities for the DM/G objects in the presence of stream velocity. As expected DM halos that host larger gas fractions are more likely to form stars, according to the $\rho_{\rm crit}$ criterion. Note that gas in the DM/G objects is expected to fragment into cooler clumps that will serve as star formation sites (e.g., Bromm et al. 1999; Greif et al. 2011).

Significantly, 88% of SIGOs may form stars for the $2\sigma_{v_{\rm bc}}$ run (there are ipso facto no SIGOs in the $v_{\rm bc} = 0$ run). As depicted in Figure 2, SIGOs have densities that are much higher than $\rho_{\rm crit}$ and are overall cool. In other words, the majority of SIGOs have supercritical densities and are thus ripe sites for star formation.

Note that because SIGOs are only marginally bound (Chiou et al. 2018), supernova feedback may disrupt the rest of the gas in them, thus suppressing further star formation. Indeed, GCs tend to have multiple generations of stars, possibly from multiple starburst epochs. Subsequent star bursts may form during pericenter passage as a SIGO orbits the closest DM halo, if gas survived the supernova feedback or was able to accrete from the medium.[10] Here we focus on the first star formation episode and hence adopt a starburst formation model.

4. SIGO and DM/G Luminosity

For the SIGOs and DM/G, with pristine gas, we follow Schaerer (2003) and consider a starburst model with no metallicity at redshift $z = 20$ (his model "A"). This includes Lyα lines and the H ionizing photon flux, Q(H). The luminosity is given by

$$L_l[\rm erg\ s^{-1}] = c_l(1 - f_{\rm esc})Q_i(t)[\rm s^{-1}], \quad (6)$$

where Q_i is the ionizing photon flux,[11] c_l is the line emission coefficient for Case B, and $f_{\rm esc}$ is the photon escape fraction. We assume a photon escape fraction of $f_{\rm esc} = 0.5$ and that 10% of the gas mass of a SIGO or a classical object (DM/G) will be converted into stars.

With these relations at hand we estimate the luminosity–mass (Figure 3) and luminosity–radius (Figure 4) relation for the different objects. As it can be clearly seen in these figures, the SIGOs and DM/G occupy different parts of the parameter space. Moreover, as shown in Figure 3, SIGOs cover the GC mass range.

As expected, and noted previously in the literature (e.g., Greif et al. 2011; Stacy et al. 2011), the stream velocity suppresses the abundance of DM/G objects and in particular

[9] This expression assumes a line width size relation with exponent of $p = 0.5$, expected for supersonic turbulence.

[10] Here we adopt a semi-analytical approach for star formation, because detailed zoom-in simulations exploring the supernova feedback are beyond the scope of this Letter.

[11] Note that following the model of Schaerer (2003), $Q_i(t)$ has a linear dependency on the mass of the object.

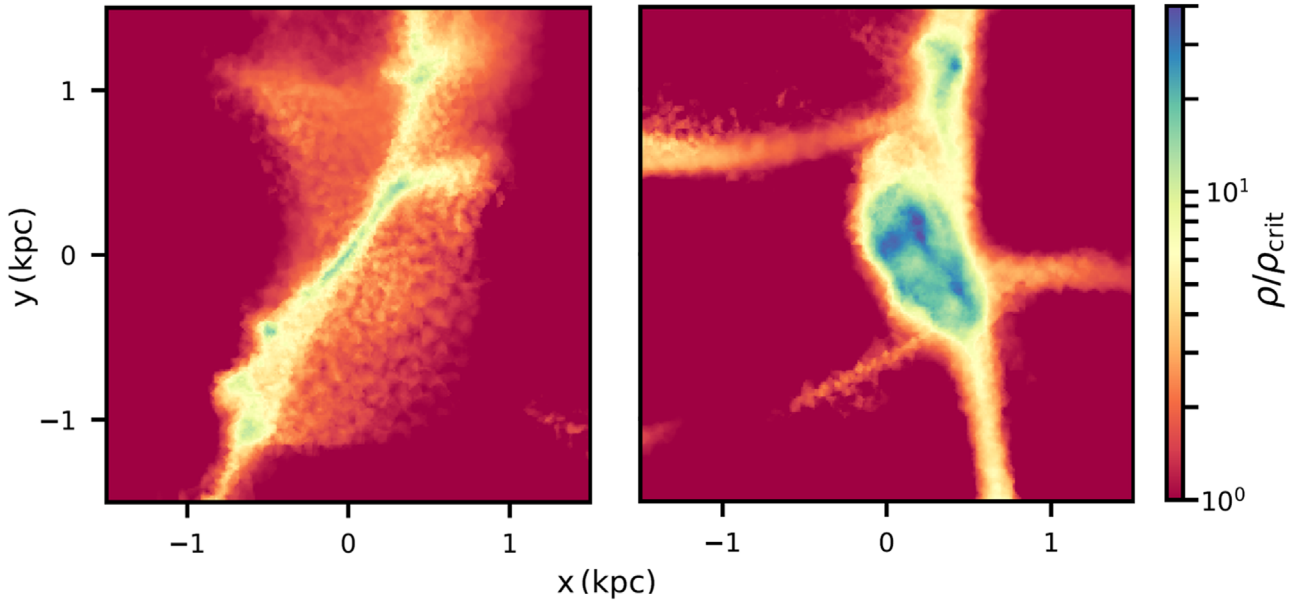

Figure 1. Density projections of two representative SIGOs at $z = 20$. The density has been normalized to ρ_{crit} for each SIGO. The highest density ratio here is ∼40, corresponding to dark blue color. Note the filamentary nature with multiple high, smaller-scale density peaks. The SIGO is embedded at the center of the region with a scale of (R_{min}, R_{max}) of (0.01, 0.03) kpc and (0.08, 0.14) kpc for the left and right panels, respectively.

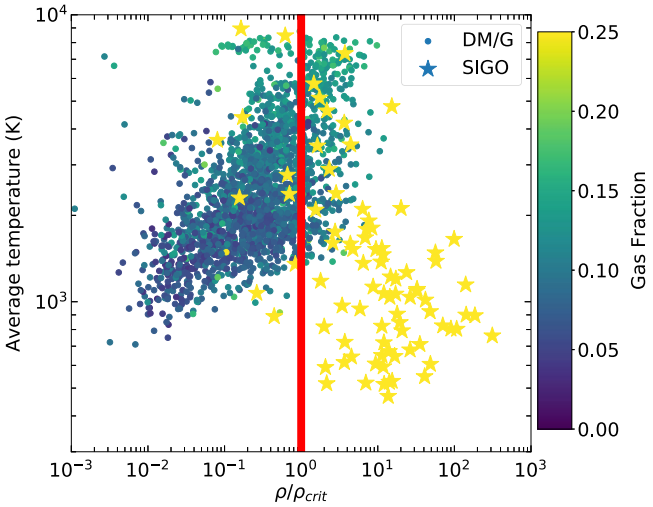

Figure 2. Average temperature in the stream velocity run as a function of ρ/ρ_{crit}, at $z = 20$. The red vertical line indicates the $\rho = \rho_{crit}$ line. To the right of the line we expect star formation to take place and to the left, star formation is suppressed. The color code depicts the gas fraction in the object. Recall that by definition SIGOs have gas fraction above 40%. Note the majority SIGOs are in the star-forming regime.

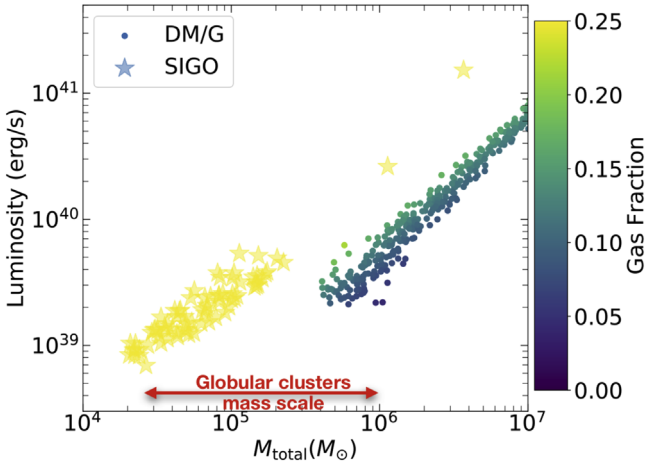

Figure 3. Luminosity as a function of mass for the $v_{bc} = 2\sigma_{v_{bc}}$ run at $z = 20$. The color code depicts the gas fraction in the object. The horizontal line represents a characteristic mass scale of present-day, local, GCs (e.g., Kimmig et al. 2015).

the star-forming ones. In Figure 4, we display the results of the runs with and without stream velocity. The left panel corresponds to the no-stream-velocity case. Here, there are no SIGOs present and there is a fairly tight relation. With stream velocity, in the right panel, there are less DM/Gs and there is more scatter in the distribution.

The SIGOs occupy a dimmer and more compact part of the parameter space. In general star formation would occur in high-density peaks that are much smaller than the size of the SIGO, therefore we consider the characteristic scale to be the smallest ellipsoid axis[12] (whereas the characteristic scale for the DM/G is simply the virial radius). Indeed, it has been argued that GCs might form as the nuclei of a dwarf galaxy that dissolved (e.g., Searle & Zinn 1978). Because luminosity is calculated based on the total gas mass of the object and SIGOs tend to be not be very massive, there is a separation in luminosity–mass space. As for luminosity–radius space, the prolate nature of SIGOs gives them a distribution of sizes and they tend to be less luminous in general than the DM/G.

The mass and characteristic scale of the SIGOs seems to be consistent with Little Blue Dots (Elmegreen & Elmegreen 2017) and the star-forming dwarf detected recently by Vanzella et al. (2019). The aforementioned observed objects have been suggested to be GCs progenitors, their similarity to SIGOs is uncanny and may suggest a strong link between high redshift, star-forming SIGOs, and GCs progenitors. Future *Hubble Space Telescope* (*HST*) and *JWST* observations may yield stronger evidence.

[12] Recall that we use R_{max} to calculate the the density threshold, because R_{max} describes the turbulence scale.

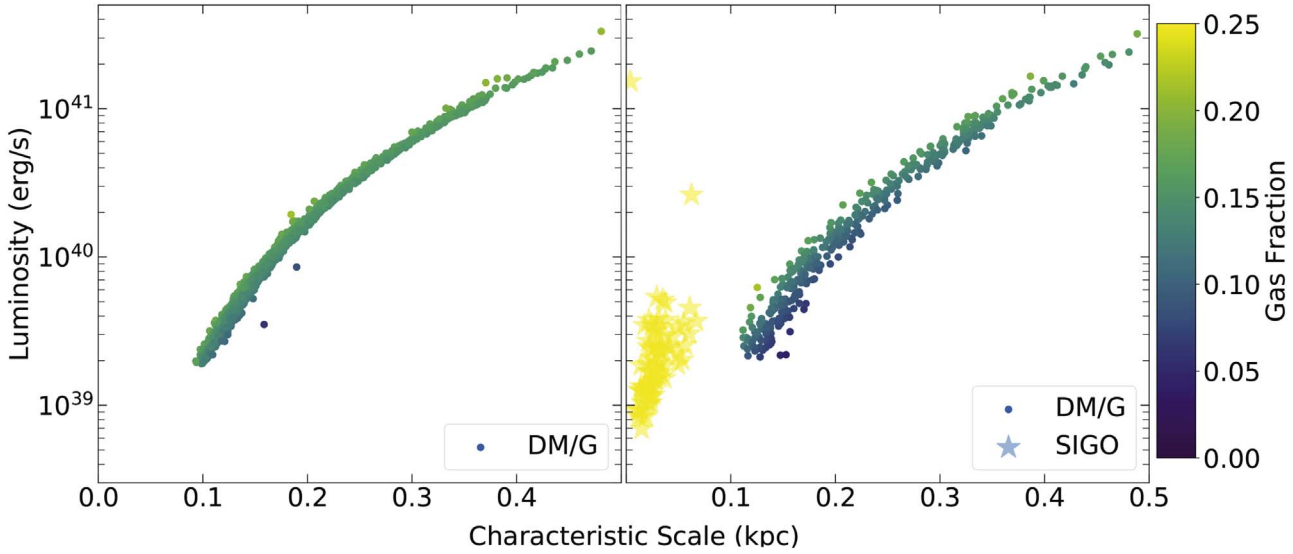

Figure 4. Luminosity as a function of the characteristic scale for $v_{bc} = 0$ (left), $2\sigma_{v_{bc}}$ (right). For the SIGOs, the characteristic scale chosen is the minimum ellipsoid axis. For DM/G objects, we adopt the virial radius. Only star-forming objects with $\rho > \rho_{crit}$ are shown.

5. Discussion

The SIGOs are expected to exists in patches of the universe with non-negligible stream velocity (Naoz & Narayan 2014; Popa et al. 2016; Chiou et al. 2018). We showed that these gas-rich objects, with little to no DM components, have high-enough densities that can give rise to star formation. Thus, the early universe is predicted to have two classes of star-forming objects, the classical ones, i.e., high gas densities within DM halos (DM/G), as well as SIGOs.

We estimated the luminosity expected from star formation in these objects (both SIGOs and the classical objects). Due to the formation nature of SIGOs, they occupy different parts of the parameter space than the classical DM halos with gas. The SIGOs are dimmer than the classical objects at the same redshift. Note that, while the simulation snapshot here is associated with $z = 20$, we expect these objects to continue to form[13] and exist (at least before reionization), based on the agreement between the analytical calculations (Naoz & Narayan 2014) and our simulations (Popa et al. 2016; Chiou et al. 2018; Y. S. Chiou et al. 2019, in preparation). Thus, future *JWST* observations may be able to disentangle star-forming SIGOs from classical objects.

Moreover, we note that the recently observed Little Blue Dots (Elmegreen & Elmegreen 2017), which are suggested to be star-forming progenitors of GCs, are consistent with with the mass and radius of SIGOs in the simulation. The star-forming dwarf found by Vanzella et al. (2019) also has a similar mass and size to our largest SIGOs. There may also be a connection between SIGOs and giant H II regions and H II galaxies (Terlevich et al. 2018). Furthermore, SIGOs that formed few to no stars may be connected to the starless dark H I objects predicted by Burkhart & Loeb (2016). Interestingly, the recent discoveries of two galaxies with little to no DM (van Dokkum et al. 2018, 2019; Danieli et al. 2019), share a striking resemblance to SIGOs. While the size estimation of these low-redshift galaxies is somewhat larger (few kpc) than the SIGOs (1–100 pc), we speculate that these objects may be a result, in the local universe, of a collections or mergers of SIGOs. Moreover, the 10 GCs identified around one of these galaxies (Danieli et al. 2019), are consistent with multiple high-density peaks we have found within our high-redshift simulated SIGOs.

The separation of SIGOs and DM/G in the luminosity–radius parameter space (e.g., Figure 3) highly resembles the magnitude–radius separation parameter space of present-day, local, GCs, and sub-groups separation (e.g., McConnachie 2012, see their Figure 6). Thus, we may speculate on how SIGOs and DM/G objects will be observed today. Assuming a burst-like star formation before reionization ($z = 10$), we adopt an initial mass function (IMF) for the objects. In particular, we adopt a top-heavy IMF for the SIGOs[14] following Decressin et al. (2007), and a Salpeter IMF for the DM/G. We then calculate the fraction of spectral types of stars that evolve along the main sequence. The majority of the stars that survive to the present day will be G and K type stars, as well as red giants. Given this population, we subtract their various bolometric corrections. We can then roughly estimate each object's visual bolometric magnitude. We also estimate that the observed stellar cluster that formed within the SIGOs corresponds to the highest density peak, which is typically smaller than R_{max}. Thus, we adopt the R_{min} for the observed value. Our order of magnitude estimations are presented in Figure 5. We also over-plot the region of the parameter space that is associated with GCs (red box) and Andromeda and the Milky Way sub-groups (blue area; McConnachie 2012). Heuristically, the SIGOs are consistent with the absolute visual magnitudes of present-day, local GCs. Although the SIGOS in this simulation only contain primordial gas, we speculate that some self-enrichment or second population-formation mechanism (such as pericenter passage of orbits about the nearest DM halo) may contribute to the nonzero metallicity in metal-poor GCs. Further simulations

[13] Note that $\sim 10^6\ M_\odot$ objects are expected to be fairly common (represent about a $1-\sigma$ fluctuation) at about $z \sim 6$ (e.g., Naoz & Barkana 2007; Fialkov et al. 2012; Barkana 2016).

[14] Following Decressin et al. (2007), we use a piecewise IMF, with low-mass end ($0.1\ M_\odot < M < 0.8\ M_\odot$) is given by a lognormal form and above $0.8\ M_\odot$ it is given by a top-heavy power law with slope $x = 0.55$. Note that using a Salpeter slope for the SIGOs' IMF did not significantly affect the results.

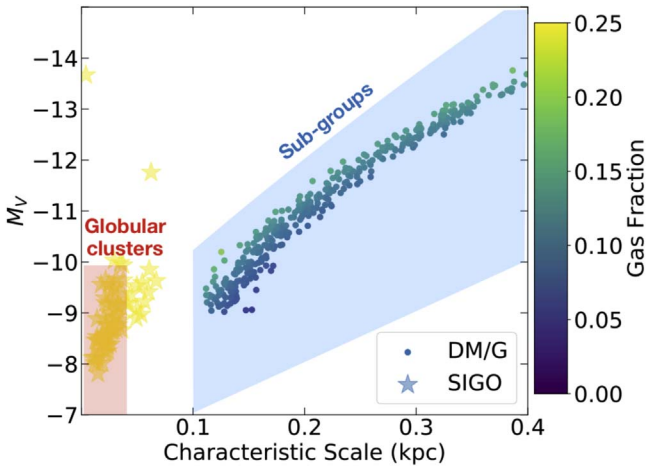

Figure 5. Speculated present-day, local, absolute visual magnitude as a function of characteristic scale of SIGOs and DM/G (see the text for details). Over-plotted are object classes in the Local Group from McConnachie (2012).

including explicit star formation (and the associated metal enrichment) are needed to address this. Nevertheless, the agreement between our rough estimates and the observations is very encouraging.

Finally, these results suggest that if this is the dominant formation mechanism of GCs, varying patches (on the order of few tens of Mpc) in the universe associated with different coherent $v_{\rm bc}$ values, will have significantly distinct abundances of GCs.[15] Indeed, about 39% of the universe contains patches of stream velocity with $v_{\rm bc} \geqslant 1\sigma_{v_{\rm bc}}$ (Tseliakhovich et al. 2011). Thus, detailed *HST* and future *JWST* observations may allow to disentangle between different formation channels of GCs.

The authors would like to thank Alice Shapley for leading UCLA GalRead, and leading enlightening discussions, in particular about GC and dwarf galaxy parameter space. We also thank Alice Shapley and Brad Hansen for useful discussions about the observations, and Steve Furlanetto and Jordon Mirocha for useful discussions about the semi-analytical calculations. We thank the anonymous referee for useful comments that improved this Letter. Y.S.C. would also like to thank Rick Mebane for useful comments. S.N. thanks Howard and Astrid Preston for their generous support. B.B. acknowledges the generous support of the Simons Foundation and discussions with Greg Bryan and Jerry Ostriker. F.M. is supported by the Program "Rita Levi Montalcini" of the Italian MIUR. M.V. acknowledges support through an MIT RSC award, a Kavli Research Investment Fund, NASA ATP grant NNX17AG29G, and NSF grants AST-1814053 and AST-1814259. Finally, we thank Volker Springel for granting us access to the AREPO code. The simulations presented here were run using Simons Foundation Flatiron Institute computational resources.

[15] From linear theory, the abundance of SIGOs on face value should follow the abundance of gas-poor DM halos (e.g., Naoz & Narayan 2014). Numerically, SIGOs undergo two-body relaxation processes and numerically evaporate, (e.g., Popa et al. 2016; Chiou et al. 2018); thus, detailed abundance studies are challenging. Note that our choice of a larger σ_8 provides higher power, which enables us to overcome some of the numerical challenges and can be viewed as a high-fluctuation patch in the universe.

ORCID iDs

Smadar Naoz https://orcid.org/0000-0002-9802-9279

References

Abel, T., Bryan, G. L., & Norman, M. L. 2002, Sci, 295, 93
Ashman, K. M., & Zepf, S. E. 1992, ApJ, 384, 50
Barkana, R. 2016, PhR, 645, 1
Bekki, K., & Yong, D. 2012, MNRAS, 419, 2063
Bonnor, W. B. 1956, MNRAS, 116, 351
Bouwens, R. J., Illingworth, G. D., Oesch, P. A., et al. 2017, arXiv:1711.02090
Boylan-Kolchin, M. 2018, MNRAS, 479, 332
Bradford, J. D., Geha, M., Muñoz, R. R., et al. 2011, ApJ, 743, 167
Bromm, V., & Clarke, C. J. 2002, ApJL, 566, L1
Bromm, V., Coppi, P. S., & Larson, R. B. 1999, ApJL, 527, L5
Bromm, V., Coppi, P. S., & Larson, R. B. 2002, ApJ, 564, 23
Burkhart, B. 2018, ApJ, 863, 118
Burkhart, B., & Loeb, A. 2016, ApJL, 824, L7
Burkhart, B., & Mocz, P. 2018, arXiv:1805.11104
Burkhart, B., Stalpes, K., & Collins, D. C. 2017, ApJL, 834, L1
Chiou, Y. S., Naoz, S., Marinacci, F., & Vogelsberger, M. 2018, MNRAS, 481, 3108
Christlieb, N., Bessell, M. S., Beers, T. C., et al. 2002, Natur, 419, 904
Conroy, C., Loeb, A., & Spergel, D. N. 2011, ApJ, 741, 72
Dalal, N., Pen, U.-L., & Seljak, U. 2010, JCAP, 11, 007
Danieli, S., van Dokkum, P., Conroy, C., Abraham, R., & Romanowsky, A. J. 2019, ApJL, 874, L12
Decressin, T., Charbonnel, C., & Meynet, G. 2007, A&A, 475, 859
Ebert, R. 1955, ZA, 37, 217
Elmegreen, B. G., Malhotra, S., & Rhoads, J. 2012, ApJ, 757, 9
Elmegreen, D. M., & Elmegreen, B. G. 2017, ApJL, 851, L44
Fialkov, A. 2014, IJMPD, 23, 1430017
Fialkov, A., Barkana, R., Tseliakhovich, D., & Hirata, C. M. 2012, MNRAS, 424, 1335
Girichidis, P., Konstandin, L., Whitworth, A. P., & Klessen, R. S. 2014, ApJ, 781, 91
Glover, S. 2013, in The First Stars, ed. T. Wiklind, B. Mobasher, & V. Bromm (Berlin: Springer), 103
Glover, S. C. O., & Jappsen, A.-K. 2007, ApJ, 666, 1
Greif, T. H., Springel, V., White, S. D. M., et al. 2011, ApJ, 737, 75
Grillmair, C. J., Freeman, K. C., Irwin, M., & Quinn, P. J. 1995, AJ, 109, 2553
Gunn, J. E. 1980, RSPTA, 296, 313
Guszejnov, D., Hopkins, P. F., Grudić, M. Y., Krumholz, M. R., & Federrath, C. 2018, MNRAS, 480, 182
Harris, W. E., & Pudritz, R. E. 1994, ApJ, 429, 177
Hartwig, T., Glover, S. C. O., Klessen, R. S., Latif, M. A., & Volonteri, M. 2015, MNRAS, 452, 1233
Heggie, D. C., & Hut, P. 1996, in IAU Symp. 174, Dynamical Evolution of Star Clusters: Confrontation of Theory and Observations, ed. P. Hut & J. Makino (Dordrecht: Kluwer), 303
Hirano, S., Hosokawa, T., Yoshida, N., & Kuiper, R. 2017, Sci, 357, 1375
Ibata, R., Nipoti, C., Sollima, A., et al. 2013, MNRAS, 428, 3648
Jeans, J. H. 1902, RSPTA, 199, 1
Kimmig, B., Seth, A., Ivans, I. I., et al. 2015, AJ, 149, 53
Krauss, L. M., & Chaboyer, B. 2003, Sci, 299, 65
Kravtsov, A. V., & Gnedin, O. Y. 2005, ApJ, 623, 650
Kruijssen, J. M. D. 2015, MNRAS, 454, 1658
Krumholz, M. R., & McKee, C. F. 2005, ApJ, 630, 250
Latif, M. A., Niemeyer, J. C., & Schleicher, D. R. G. 2014, MNRAS, 440, 2969
Maio, U., Koopmans, L. V. E., & Ciardi, B. 2011, MNRAS, 412, L40
Mandelker, N., van Dokkum, P. G., Brodie, J. P., van den Bosch, F. C., & Ceverino, D. 2018, ApJ, 861, 148
Mashchenko, S., & Sills, A. 2005, ApJ, 619, 243
McConnachie, A. W. 2012, AJ, 144, 4
McQuinn, M., & O'Leary, R. M. 2012, ApJ, 760, 3
Moore, B. 1996, ApJL, 461, L13
Muratov, A. L., & Gnedin, O. Y. 2010, ApJ, 718, 1266
Naoz, S., & Barkana, R. 2005, MNRAS, 362, 1047
Naoz, S., & Barkana, R. 2007, MNRAS, 377, 667
Naoz, S., Barkana, R., & Mesinger, A. 2009, MNRAS, 399, 369
Naoz, S., & Narayan, R. 2014, ApJL, 791, L8
Naoz, S., Yoshida, N., & Barkana, R. 2011, MNRAS, 416, 232
Naoz, S., Yoshida, N., & Gnedin, N. Y. 2012, ApJ, 747, 128
Naoz, S., Yoshida, N., & Gnedin, N. Y. 2013, ApJ, 763, 27

O'Leary, R. M., & McQuinn, M. 2012, ApJ, 760, 4
Peebles, P. J. E. 1984, ApJ, 277, 470
Popa, C., Naoz, S., Marinacci, F., & Vogelsberger, M. 2016, MNRAS, 460, 1625
Reed, D. S., Bower, R., Frenk, C. S., et al. 2005, MNRAS, 363, 393
Renaud, F., Agertz, O., & Gieles, M. 2017, MNRAS, 465, 3622
Richardson, M. L. A., Scannapieco, E., & Thacker, R. J. 2013, ApJ, 771, 81
Saitoh, T. R., Koda, J., Okamoto, T., Wada, K., & Habe, A. 2006, ApJ, 640, 22
Sarmento, R., Scannapieco, E., & Cohen, S. 2018, ApJ, 854, 75
Schaerer, D. 2003, A&A, 397, 527
Schaerer, D., & Charbonnel, C. 2011, MNRAS, 413, 2297
Schauer, A. T. P., Glover, S. C. O., Klessen, R. S., & Ceverino, D. 2019, MNRAS, 484, 3510
Schauer, A. T. P., Regan, J., Glover, S. C. O., & Klessen, R. S. 2017, MNRAS, 471, 4878
Searle, L., & Zinn, R. 1978, ApJ, 225, 357
Springel, V. 2010, MNRAS, 401, 791
Stacy, A., Bromm, V., & Loeb, A. 2011, ApJL, 730, L1
Tanaka, T. L., & Li, M. 2014, MNRAS, 439, 1092
Tanaka, T. L., Li, M., & Haiman, Z. 2013, MNRAS, 435, 3559
Taylor, M. A., Puzia, T. H., Gomez, M., & Woodley, K. A. 2015, ApJ, 805, 65
Terlevich, E., Fernández-Arenas, D., Terlevich, R., et al. 2018, MNRAS, 481, 268
Trenti, M., Padoan, P., & Jimenez, R. 2015, ApJL, 808, L35
Tseliakhovich, D., Barkana, R., & Hirata, C. M. 2011, MNRAS, 418, 906
Tseliakhovich, D., & Hirata, C. 2010, PhRvD, 82, 083520
van Dokkum, P., Danieli, S., Abraham, R., Conroy, C., & Romanowsky, A. J. 2019, ApJL, 874, L5
van Dokkum, P., Danieli, S., Cohen, Y., et al. 2018, Natur, 555, 629
Vanzella, E., Calura, F., Meneghetti, M., et al. 2017, MNRAS, 467, 4304
Vanzella, E., Calura, F., Meneghetti, M., et al. 2019, MNRAS, 483, 3618
Vanzella, E., De Barros, S., Cupani, G., et al. 2016, ApJL, 821, L27
Visbal, E., Barkana, R., Fialkov, A., Tseliakhovich, D., & Hirata, C. M. 2012, Natur, 487, 70
Vogelsberger, M., Genel, S., Sijacki, D., et al. 2013, MNRAS, 436, 3031
Xu, H., Norman, M. L., O'Shea, B. W., & Wise, J. H. 2016, ApJ, 823, 140
Yoshida, N., Omukai, K., Hernquist, L., & Abel, T. 2006, ApJ, 652, 6